NJC

Accepted Manuscript

This is an *Accepted Manuscript*, which has been through the Royal Society of Chemistry peer review process and has been accepted for publication.

Accepted Manuscripts are published online shortly after acceptance, before technical editing, formatting and proof reading. Using this free service, authors can make their results available to the community, in citable form, before we publish the edited article. We will replace this *Accepted Manuscript* with the edited and formatted *Advance Article* as soon as it is available.

You can find more information about *Accepted Manuscripts* in the Information for Authors.

Please note that technical editing may introduce minor changes to the text and/or graphics, which may alter content. The journal's standard Terms & Conditions and the Ethical guidelines still apply. In no event shall the Royal Society of Chemistry be held responsible for any errors or omissions in this *Accepted Manuscript* or any consequences arising from the use of any information it contains.

ROYAL SOCIETY OF CHEMISTRY

www.rsc.org/njc

Cite this: DOI: 10.1039/c0xx00000x

www.rsc.org/xxxxxx

ARTICLE TYPE

Hierarchical $CoNiO_2$ structures assembled by mesoporous nanosheets with tunable porosity and their application as lithium-ion battery electrodes

Yanguo Liu [a, †], Yanyan Zhao [b, †], Yanlong Yu [c], Jinpeng Li [d], Mashkoor Ahmad [e, *], Hongyu Sun [b, *]

Received (in XXX, XXX) Xth XXXXXXXXX 200X, Accepted Xth XXXXXXXXX 200X

DOI: 10.1039/b000000x

Mesoporous $CoNiO_2$ hierarchical structures with various specific surface area and pore size distribution were successfully synthesized by a hydrothermal method and subsequent annealing process. Structural and compositional analysis indicated that the hierarchical structures were assembled with single-crystal nanosheets. The as-prepared sample used as an anode materials of Li-ion batteries, delivered reasonable capacity, good cycling stability and rate capability. It has been found that the specific surface area and pore nature of $CoNiO_2$ hierarchical structures have strong influences on their electrochemical performances. The optimal sample delivered a high reversible lithium storage capacity of ~449.3 $mAhg^{-1}$ after 50 cycles with high Coulombic efficiency at a current rate of 0.1 Ag^{-1}, with good cycling stability and rate capability. It is believed that the improved electrochemical performance can be attributed to the mesoporous nature and the 3D assembledd electrode structure. Therefore, such mesoporous hierarchical structures can be considered to be an attractive candidate as an anode material for LIBs.

1. Introduction

Rechargeable lithium-ion batteries (LIBs) have been widely used in portable electronics, mobile phones, and laptop computers due to their advantages of high energy density, long cycling life, and environmental benignity.[1, 2] It is widely accepted that the overall performance of LIBs is highly dependent on the inherent properties of the electrode materials.[3, 4] Typical transition metal oxides (TMOs), such as Fe_2O_3, Co_3O_4, and NiO, have been widely studied as alternative conversion negative electrode materials for LIBs because of their higher discharge capacities compared to that of conventional carbon negative electrode materials.[5] However, large volume expansion and severe particle aggregation associated with the Li^+ insertion and extraction process lead to electrode pulverization and loss of particle contact, consequently, result in a large irreversible capacity loss and poor cycling stability.[6, 7] One feasible approach to overcome these drawbacks is design and synthesis of electrode materials with reasonable composition, morphology, microstructure, and architecture on the nanoscale.[3-7] In particular, hierarchical structures, which assembled by nanoscale primary building blocks (e.g., nanoparticles, nanorods, and nanosheets) with porous characteristic, have drawn special interest.[8] It is anticipated that such hierarchical structures not only well inherit the advantages from the single components but also arise novel properties due to the synergistic interactions between the nano building blocks.[9, 10] Moreover, porosity from the hierarchical structures generally leads to improved energy density, better capacity retention and superior rate capability, which are due to the large surface area, numerous active sites, short mass and charge diffusion distance, and efficient accommodation of volume changes during the charging and discharging process.[8, 11, 12] Compared to the binary TMOs, ternary counterparts with two different metal cations, have received much attention in recent years due to their promising roles in LIBs, supercapacitors, and fuel cells.[13-23] The coupling of two metal species could render the ternary metal oxides with richer redox reactions and improved electronic conductivity, which are beneficial to electrochemical applications. Besides, the various combinations of the cations and the tunable stoichiometric/non-stoichiometric compositions in the ternary metal oxides provide vast opportunities to manipulate the physical/chemical properties.[13] Recently, nickel cobalt oxide (mainly $NiCo_2O_4$) has been studied as a high-performance electrode material for energy-related applications, especially in the fields of electrochemical supercapacitors.[24-29] However, little attention has been paid to nickel cobalt oxides with compositions other than $NiCo_2O_4$ and the applications as anode materials for LIBs.[13] in particular, nickel cobalt oxide hierarchical structures with tunable specific surface area, pore size and distribution, which would greatly benefit the performance in electrochemical application, have not been fully investigated.

In this work, we report a facile synthesis of $CoNiO_2$ hierarchical structures with various specific surface area and pore size distribution and study their influences on the electrochemical performance for LIBs. The optimal sample delivered a high reversible lithium storage capacity of ~449.3 $mAhg^{-1}$ after 50 cycles with high Coulombic efficiency at a current rate of 0.1 Ag^{-1}, and showed good cycling stability and rate capability. The hierarchical structures with reasonable porous nature are responsible for the good lithium-storage properties.

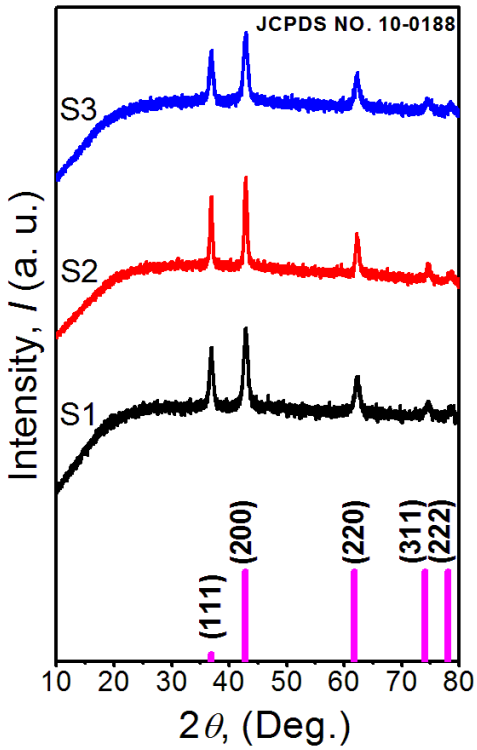

Fig.1 XRD pattern of as-prepared samples (S1, S2, and S3) and standard pattern of cubic $NiCoO_2$ phase.

2. Experimental section

2.1 Synthesis of single-crystal mesoporous $CoNiO_2$ nanosheets assembled hierarchical structures

Single-crystal mesoporous $CoNiO_2$ nanosheets assembled hierarchical structures were synthesized by a hydrothermal method and subsequent annealing process. In a typical synthesis, 1.45 g of $Co(NO_3)_2{\cdot}6H_2O$, 0.727 g of $Ni(NO_3)_2{\cdot}6H_2O$ and 1.4 g of hexamethylenetetramine (HMT) were dissolved in 30 ml of ethanol (EtOH)-water solution with different volume ratios under stirring. After stirring for 30 min, the homogeneous solution was transferred into a Teflon-linked stainless steel autoclave. The autoclave was sealed and maintained at 95 °C for 8 h. After cooling down to room temperature spontaneously, the precursor is rinsed with distilled water and ethanol, and dried at 80 °C under vacuum for 2 h. Finally, the product was annealed at 450 °C in Ar atmosphere for 2 h.

2.2 Sample characterization

The morphology and crystal structure of the products were examined by employing field-emission scanning electron microscopy equipped with an Energy Dispersive X-ray (EDX) system (FESEM; Hitachi, S5500), transmission electron microscopy (TEM; FEI, Tecnai G^2 20, 200 kV; JEOL, JEM-2011, 200 kV), X-ray photospectroscopy (XPS, Escalab 250, Al K_α), and thermal gravimetric (TG) analysis (Netzsch-STA449C, measured from room temperature to 500 °C at a heating rate of 10 °C/min under an air atmosphere). Crystallographic information for the samples was collected using a Bruker Model D8 Advance X-ray powder diffractometer (XRD) Cu-K_α irradiation (λ=1.5418 Å). The

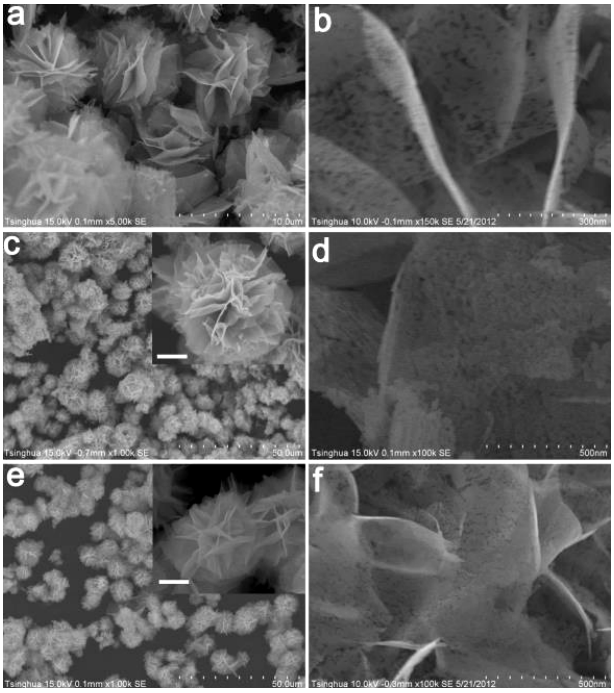

Fig.2 FESEM images of the mesoporous $CoNiO_2$ hierarchical structures with different magnifications. (a, b) S1, (c, d) S2, (e, f) S3. The scale bars in the inserts are 2 um.

Bruauer–Emmett–Teller (BET) surface area of the powders was analyzed by nitrogen adsorption-desorption isotherm measurement at 77 K in a Micromeritics ASAP 2010 system. The sample was degassed at 180 °C before nitrogen adsorption measurements. The BET surface area was determined by a multipoint BET method. A desorption isotherm was used to determine the pore size distribution via the Barret-Joyner-Halender (BJH) method, assuming a cylindrical pore model. The nitrogen adsorption volume at the relative pressure (P/P_0) of 0.994 was used to determine the pore volume and average pore size.

2.3 Cell assembly and electrochemical testing

To measure the electrochemical performance, composite electrodes were constructed by mixing the active materials, conductive carbon black and polyvinylidene fluoride (PVDF) with a weight ratio of 80 : 10 : 10. The active materials used for cells assembly are 4.16, 4.32, and 3.92 mg for S1, S2, and S3, respectively. The mixture was prepared as a slurry in N-methylpyrrolidinone and spread onto copper foil by using the doctor-blade technique. The electrode was dried under vacuum at 120 °C for 5 h to remove the solvent before pressing. Then the electrodes were cut into disks (12 mm in diameter) and dried at 100 °C for 24 h in vacuum. The cells were assembled inside an Ar-filled glove box by using a lithium-metal foil as the counter electrode and the reference electrode and microporous polypropylene as the separator. The electrolyte used was 1 M LiPF6 in ethylene carbonate (EC)-dimethyl carbonate (DMC) solvent (1: 1 w/w). Assembled cells were allowed to soak overnight, and then electrochemical tests on a LAND battery testing unit were performed. The cells were

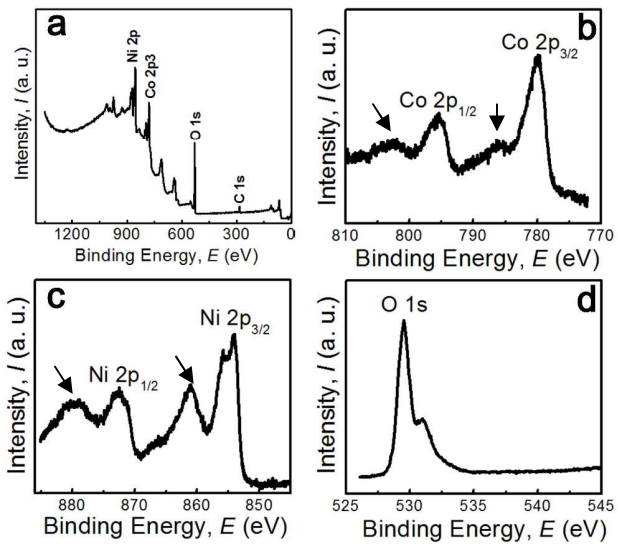

Fig.3 (a) XPS survey spectra of mesoporous $CoNiO_2$ microflowers; (b-d) high-resolution XPS spectra of the Co2p, Ni2p, and O1s regions, for S2 sample (the results for S1 and S3 are similar).

galvanostatically charged and discharged in a current density range of 0.1 Ag-1 within the voltage range of 0.01-3 V (vs. Li+/Li) for 50 cycles. For the high rate testing, the discharge current gradually increased from 0.1 Ag-1 to 0.5, 1, and 5 Ag-1, then decreased to 0.1 Ag-1, step by step. All the charge/discharge testings were performed symmetrically at room temperature.

3. Results and discussion

The morphologies and chemical composition of the as prepared precursors from various volume ratios of EtOH to water were checked by FESEM (Fig. S1†). Fig. S1a shows a typical FESEM image of the precursors synthesized in the 30 ml water solution (EtOH to water volume ratio 0/30) containing $Co(NO_3)_2{\cdot}6H_2O$, $Ni(NO_3)_2{\cdot}6H_2O$, and HMT. It can be seen that monodisperse flower-like microspheres with uniform size and morphology are obtained with a facile hydrothermal reaction. Higher magnification FESEM image show that the hierarchical structures are composed of two-dimensional (2D) thin sheets with flat and smooth surface (the inset of Fig. S1a†). EDX analysis (results not shown here) shows that the precursor is composed of Ni, Co, and O. When the volume ratio of EtOH to water increased to 10/20 and 20/10, the morphology of the flower-like microspheres is unchanged, as is clear from Fig. S1b, c. The above precursor obtained from different ratios of EtOH to water (0/30, 10/20, and 20/10) were annealed at 450 °C in Ar atmosphere for 2 h, and the obtained products are denoted as S1, S2, and S3, respectively.

The crystal structures of the yielding products were characterized by XRD as shown in Fig. 1. All of the identified peaks of the three samples are similar, and can be perfectly indexed to cubic $CoNiO_2$ (JCPDS No. 10-0188) without peaks of impurities, indicating the phase-pure nature of the products. Moreover, the relatively high peak intensities imply that the products are highly crystalline.

The morphologies of cubic $CoNiO_2$ hierarchical structures are checked by FESEM as shown in Fig. 2. In general, the final products which consist of microspheres are uniformly distributed on the substrate. Moreover, the final products inherit the original morphologies of the precursors after annealing process, which also present flower-like microspheres characteristic, indicating the robustness of the structure. The hierarchical microspheres are all assembled by 2D thin nanosheets with average thickness ~20 nm. Meanwhile, higher magnification FESEM images show that the surface of the nanosheets becomes coarse and porous, which suggests a highly porous texture (Fig. 2b, d, f). EDX results (Fig. S2†) indicate that all of the three samples are composed of Ni, Co, and O with atomic ratio about ~1:1:2 for Ni, Co to O, confirming the formation of $CoNiO_2$. Quantitative analysis confirms the Co/Ni atomic ratio about 0.98, 1.04 and 1.03 for samples S1, S2 and S3 respectively. The chemical composition of $CoNiO_2$ hierarchical structures has been analyzed by XPS analysis. Figure 3a shows the XPS survey spectrum in which Co, Ni, O and C peaks can be clearly observed. The high resolution scan of Co2p of the composite (Fig. 3b) exhibits two peaks located at 795.3 and 779.9 eV corresponding to the electronic states of $Co2p_{1/2}$ and $Co2p_{3/2}$ respectively, and the presence of shakeup satellite peaks (arrows in b) indicates the electronic state of only Co^{2+}.[30-32]. The spectrum in Fig. 3c shows that the peaks at the binding energies of 853.9 and 872.9 eV, could be assigned to Ni $2p_{3/2}$ and Ni $2p_{1/2}$ respectively, characteristic of only Ni^{2+}.[33, 34] The arrows in (c) show satellite peaks of Ni $2p_{1/2}$, and Ni $2p_{3/2}$.The Ni2p peak in the spectrum clearly indicates the existence of Ni element in the structure. The presence of $CoNiO_2$ in the composite can be further confirmed by the O1s peak (Fig. 3d) located at 530.2 eV, which correspond to the oxygen species in the $CoNiO_2$ phase. The shoulder in O1s peak in the binding energy spectrum indicate the presence of residual oxygen containing groups such as -OH and C-O.

The detailed structural investigations of the $NiCoO_2$ hierarchical structures are studied by TEM and HRTEM. Fig. 4a1-a2 are typical TEM images for S1 with different magnifications, it can be seen that the consisted building blocks of the hierarchical structures, thin nanosheets, are highly porous, which are consistent with the FESEM observations. Moreover, the porous nanosheets consist of interconnected nanoparticles. The size of these nanoparticles is in the range of 10-30 nm. The corresponding selected area electron diffraction (SAED) pattern further confirms that the as obtained hierarchical structure is single-crystal in nature with the zone axis being [110] as shown in the inset of Fig. 4a2. Fig. 4a3 shows a typical HRTEM image of an individual $NiCoO_2$ nanosheet from the microflowers. The lattice spacings of d ~ 2.14 Å and 2.45 Å are determined (see Fig. 4a3), which correspond to the (200) and (111) planes of cubic $NiCoO_2$, respectively. The measured angle between the (200) and (111) planes is about □ =55.3°, which is in agreement with the calculated value □ = 54.7°. These results undoubtedly demonstrate that we succeeded in obtaining cubic $CoNiO_2$ hierarchical structures assembled with single-crystal mesoporous nanosheets. TEM and HRTEM results for S2 (Fig. 4b1-b4) and S3 (Fig. 4c1-c4) possess similar structural features with S1, *i.e.*, cubic $CoNiO_2$ hierarchical structures composed of single-crystal mesoporous nanosheets building blocks. The formation of mesoporous structures can be ascribed to the decomposition of the precursors and the subsequent annealing process, during which the gaseous species released assist in

Cite this: DOI: 10.1039/c0xx00000x

www.rsc.org/xxxxxx

ARTICLE TYPE

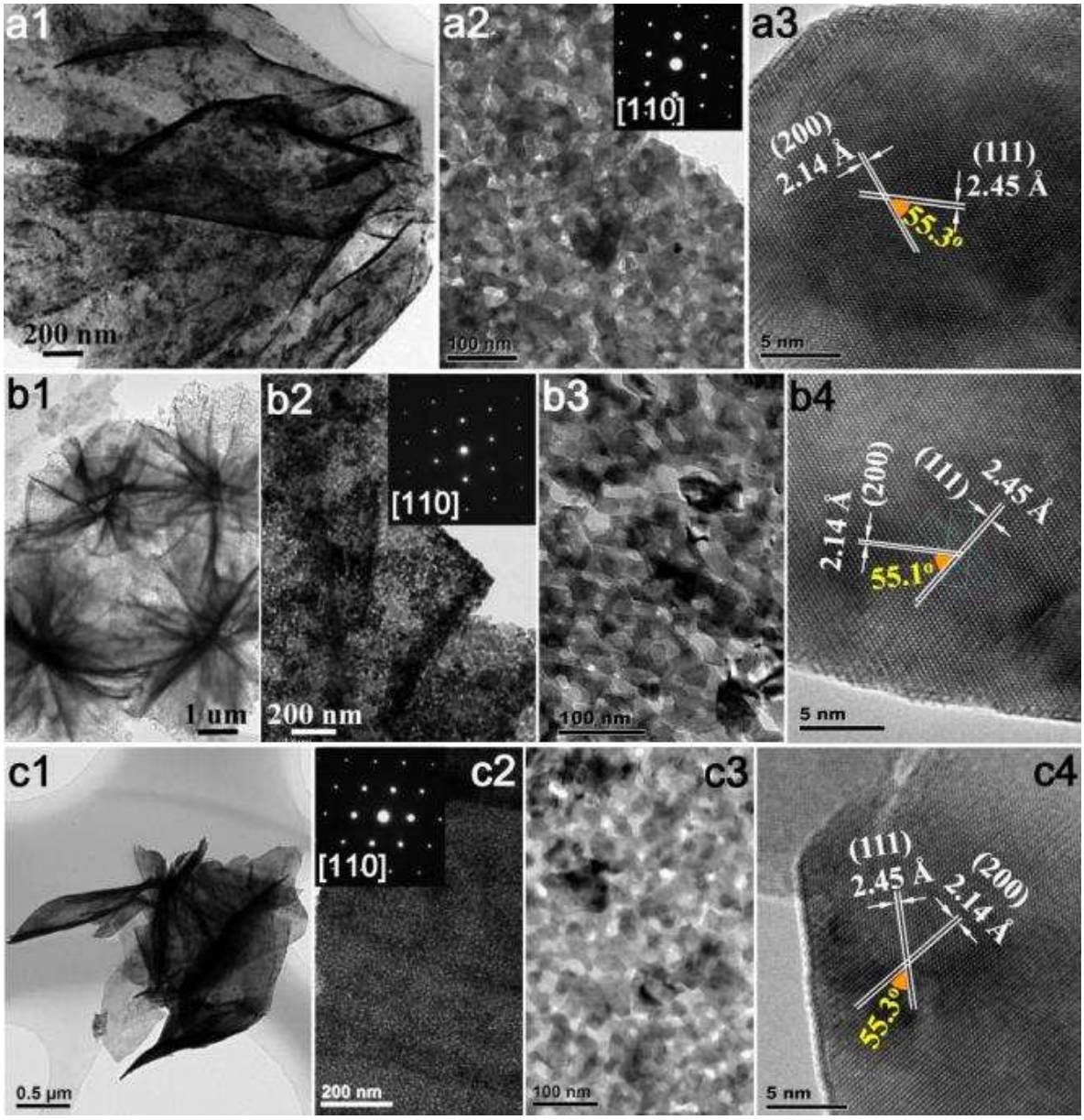

Fig.4 TEM and HRTEM images of the mesoporous $CoNiO_2$ hierarchical structures: (a1-a3) S1, (b1-b4) S2, (c1-c4) S3. The insets in (a2, b2 and c2) are corresponding SAED patterns.

constructing the highly porous texture. As a result, abundant mesopores between the nanoparticles are generated throughout the whole $CoNiO_2$ hierarchical structures. It should be mentioned here the size of the constituted nanoparticles for S1, S2, and S3 is similar, however, the pores size and their distributions are different for the threes samples from the above TEM observations. In order to further study the pore structures of the $CoNiO_2$ hierarchical structures, the specific surface areas and the porous nature of the samples are determined by measuring nitrogen adsorption-desorption isotherms at 77K (Fig. 5a). The BET specific surface area is 28.8, 44.1, and 79.6 m^2/g for S1, S2, and S3, respectively, which indicates that the specific surface area increases with the increasing of EtOH volume during the synthesis of precursors. In addition, the

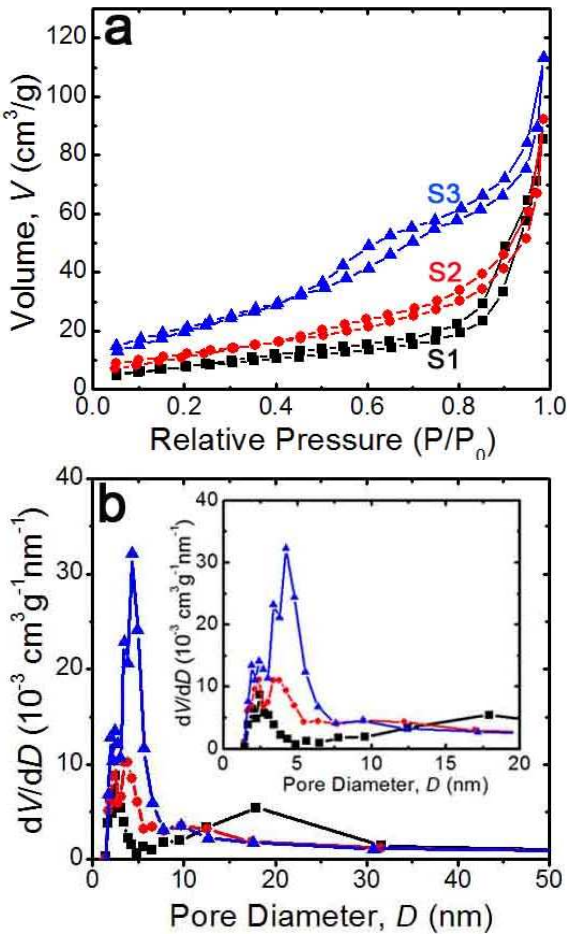

Fig.5 (a) Nitrogen adsorption-desorption isotherms and (b) corresponding pore size distribution curves of the mesoporous $CoNiO_2$ hierarchical structures.

mesopore size distributions based on BJH method of all the three samples are further confirmed by the corresponding pore size distributions curves (Fig. 5b). These results show that the $CoNiO_2$ hierarchical structures have large surface areas which are due to the mesoporous nature of the assembled nanosheets and the void spaces between the nanosheets. Nevertheless, the three samples show some difference in their porous structures. With the increasing of EtOH volume in the precursors, the amount of mesopores within the range of around 2-7 nm increased accordingly. The present hierarchical mesoporous $CoNiO_2$ structures are of importance in lithium-storage processes, due to their capability of providing extra active sites for the storage of lithium ions and facilitating mass diffusion and ion transport, which are induced by their mesoporous structures. Hence, the different porous structures of the three samples may affect their performance in lithium-storage, just like porous textures have important influence on the supercapacitive performance.

The electrochemical properties of the hierarchical mesoporous $CoNiO_2$ structures as the anode material for lithium-ion batteries are studied. To evaluate the lithium storage performance, coin cells are assembled by using $CoNiO_2$ structures as anode for LIBs. The electrochemical detail of the assembled cell is investigated by conducting voltammetric experiments at a scan rate of 1 mV/s between 0.05 and 3 V (verses Li+/Li) at room temeperature. Figure 6(a) shows the first three cyclic voltammograms (CVs) for S2 sample. In the first cycle, there are two reduction peaks at voltage positions of 0.42 and 0.63 V during the cathodic process, which can be assigned to the initial reduction of Co^{2+} to Co, and Ni^{2+} to Ni and the formation of amorphous Li_2O, as well as a partially irreversible solid electrolyte interphase (SEI) layer.[31, 35-38] In the subsequent anodic process the anodic peak at ~2.15 V is ascribed to the decomposition of Li_2O and the formation of Co^{2+} and Ni^{2+}. Compare to the initial cycle, in the second and third cycles, a decrease in the reduction peak intensity could be observed with a shift to a higher potential at about 0.99 and 1.06 V, which might be related to the pulverization of the $CoNiO_2$. The peaks intensity and the integral areas of the third cycle are very close to that of second cycle. These results show that the electrochemically reversibility of the $CoNiO_2$ electrode is gradually improve after the first cycle. In the subsequent cycles, the CV curves exhibit excellent reproducibility and almost no change in the peak shape is observed, suggesting high reversibility of the $CoNiO_2$ electrode.[39]

Fig. 6b shows the voltage capacity profiles of the three samples for the first charge/discharge cycle at a current rate of 0.1 Ag-1 in the voltage range of 0.01-3 V(vs. Li+/Li), in which all three electrodes display similar electrochemical behaviors. One dominant potential plateau at 0.63-0.7 V can be observed in the discharge process, while potential plateaus at 2.0-2.26 are shown in the charge process. It can be seen that the initial discharge and charge capacities are 865.1 and 433.4 mAhg-1 for S1, 941.3 and 617.1 mAhg-1 for S2, and 963.2 and 553.9 mAhg-1 for S3, yielding irreversible capacity losses of 49.9%, 34.4%, and 42.5%, respectively. Such initial irreversible capacity loss should mainly originate the formation of SEI layer due to the irreversible degradation of electrolyte and other secondary reactions, which is common for metal oxide electrode materials.

The comparison of cycling performance of the three samples at a current rate of 0.1 Ag^{-1} up to 50 cycles is presented in Fig. 6c. It can be seen that after the first several cycles the $CoNiO_2$ hierarchical structures show good cyclic capacity retention during cycling. It is obvious that the S3 cell is superior, with the highest lithium storage capacity. The reversible capacity reaches ~449.3 $mAhg^{-1}$ after 50 cycles with Coulombic efficiency of 97%. In comparison, the reversible capacity of S2 cell decreases to ~397.4 $mAhg^{-1}$ with a Coulombic efficiency of 96 % after 50 cycles of operation, and the reversible capacity of S1 cell drops down to ~320.7 $mAhg^{-1}$.

As rate capability is an important parameter for batteries applications, we also investigated the electrochemical performance of the three samples at various rates between 0.1 Ag^{-1} and 5.0 Ag^{-1} as shown in Fig. 6d. The charge/discharge rates are programmably modified from 0.1 Ag^{-1} to 0.5 Ag^{-1}, 1.0 Ag^{-1}, 5.0 Ag^{-1} and then back to 0.1 Ag^{-1} for 10 cycles. It can be observed that the reversible capacity of S3 cell varies from 963.9 $mAhg^{-1}$ to 66 mAhg-1 at current rates of 0.1 Ag^{-1} and 5.0 Ag^{-1}, respectively. However, the reversible capacity of the S1 and S2 cells rapidly drops from 888 to 25 $mAhg^{-1}$ and 940 to 42 $mAhg^{-1}$ respectively. When the rate return to the initial 0.2C after 40 cycles, S1 composite cell recovers its original capacity a little bit lower (450 $mAhg^{-1}$ for the 50th cycle). The morphology and structure of the mesoporous $CoNiO_2$ hierarchical structured electrodes after rate capability testing (50 cycles) are characterized by SEM and TEM (Fig. S3†). It

Cite this: DOI: 10.1039/c0xx00000x

www.rsc.org/xxxxxx

ARTICLE TYPE

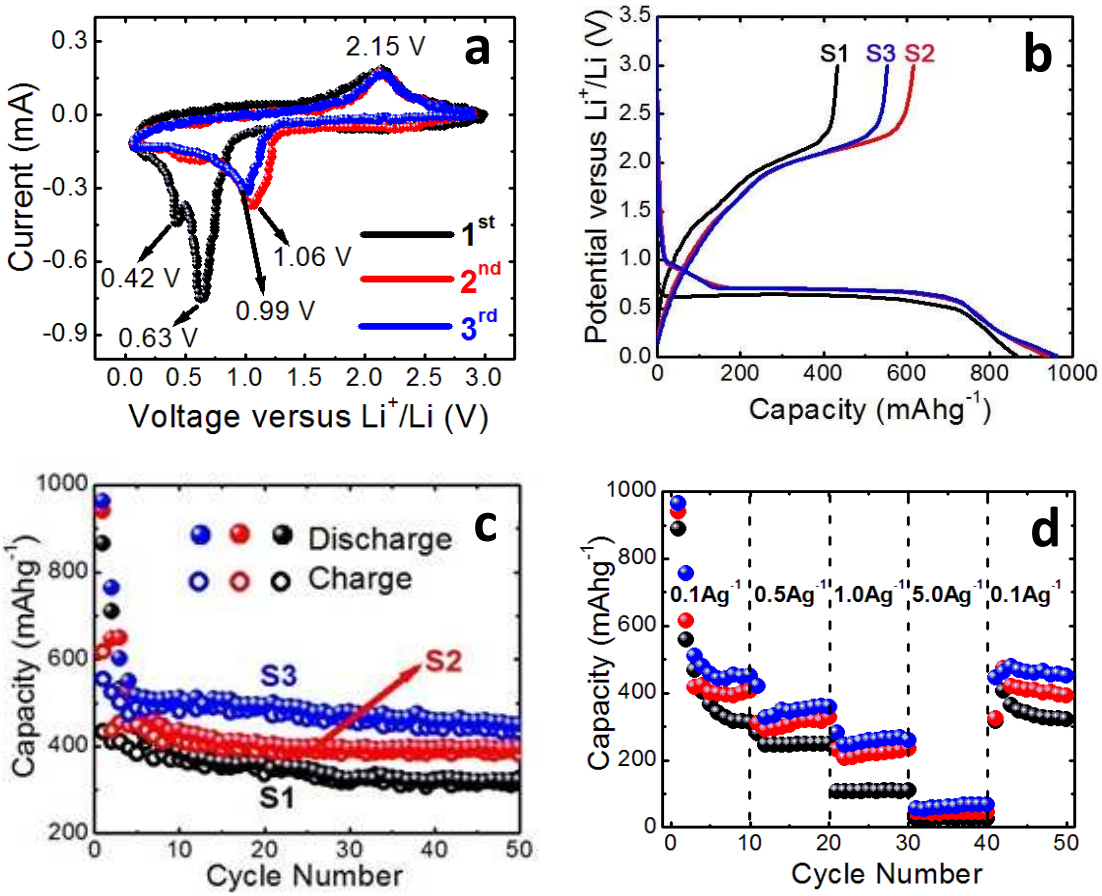

Fig.6 (a) Cyclic voltammograme of $CoNiO_2$ hierarchical structured electrode (sample S2) at a scan rate of 0.1 mVs^{-1} (b) Charge/discharge curves of the first cycle of the mesoporous $CoNiO_2$ hierarchical structured electrodes (S1, S2, and S3) at a charge/discharge rate of 0.1 Ag^{-1}. (c) The cycling performance of the mesoporous $CoNiO_2$ hierarchical structured electrodes (S1, S2, and S3) at a charge/discharge rate of 0.1 Ag^{-1}. (d) Cycling performance of the mesoporous $CoNiO_2$ hierarchical structured electrodes (S1, S2, and S3) at various current rates.

can be seen that all of the three samples still maintain the initial flower-like morphologies after cycling testing. HRTEM images demonstrate that the assembled nanosheets are still highly crystalline. The results reveal the good structural and morphological stabilities of mesoporous $CoNiO_2$ hierarchical structures during charge/discharge cycling.

The electrochemical measurements show that the $CoNiO_2$ hierarchical structures possess good lithium-storage properties in terms of specific capacity, rate capability, and cycling stability. In particular, the S3 sample shows the best lithium-storage performance among the investigated samples. There are several possible reasons which may be responsible for the superior Li-battery performance of the $CoNiO_2$ hierarchical electrode materials. (1) The 3D hierarchical architecture assembled with single-crystal nanosheets is favored for preventing the undesirable aggregation of these nano/microcrystals and ensure the stability of the porous structure, which are of importance for the cycling stability. (2) The mesoporous structures can accommodate the local volume change upon charge/discharge cycling and is able to alleviate the problem of pulverization and aggregation of the electrode material, hence improving the cycling performance. (3) The mesoporous $CoNiO_2$ hierarchical structures can provide extra active sites for the storage of lithium ions, which is beneficial for enhancing the specific capacity. (4) The mesoporous structures can reduce the effective diffusion distance for lithium ions and electrons, resulting in good rate capabilities. Therefore, abundant mesopores and large specific surface area are of great importance for the lithium-storage properties, which is the main reason that S3 sample with abundant mesopores shows superior performance. On the basis of the above analyses, it is suggested that the hierarchical mesoporous structures are responsible for the excellent electrochemical performance, which can be further improve by optimizing the pore structures and distributions. On the other hand, the present

route to hierarchical mesoporous structures can be extended to synthesis other functional metal oxides with desirable nanostructures and various functions.

Conclusions

In conclusion, mesoporous $CoNiO_2$ hierarchical structures with various specific surface area and pore size distribution, assembled with single-crystal nanosheets, were successfully synthesized by a hydrothermal method and subsequent annealing process. It has been found that the porosity of the products can be tuned by controlling the EtOH volume ratio and the specific surface area increases with the increase in EtOH volume during the synthesis of precursors. The as-prepared sample delivered reasonable capacity, good cycling stability and rate capability. The specific surface area and porous nature of $CoNiO_2$ hierarchical structures have strong influences on their electrochemical performances. The optimal sample delivered a high reversible lithium storage capacity and showed good cycling stability and rate capability. It is believed that the improved electrochemical performance can be attributed to the mesoporous nature and the 3D assembled electrode structure. The present results also show the importance of pore structure control for the electrochemical performance. We suggest to synthesize electrode materials with suitable mesoporous hierarchical structures to improve their electrochemical performance.

Acknowledgment

The authors would like to appreciate the financial supports from China Postdoctoral Science Foundation (20110490024). This work made use of the resources of the Beijing National Center for Electron Microscopy.

Notes and references

[a] *School of Resources and Materials, Northeastern University at Qinhuangdao, Qinhuangdao 066004, P. R. China*

[b] *School of Material Science and Engineering, Tsinghua University, Beijing 100084, P. R. China*

[c] *Department of Petrochemical, Northeast Petroleum University at Qinhuangdao, Qinhuangdao 066004, P. R. China*

[d] *Department of Applied Physics, Waseda University, Tokyo, 169-8555, Japan*

[e] *Nanomaterials Research group (NRG), Physics Division, PINSTECH, P.O. Nilore, Islamabad 44000, Pakistan*

*Corresponding authors emails: mashkoorahmad2003@yahoo.com

† Electronic Supplementary Information (ESI) available: [details of any supplementary information available should be included here]. See DOI: 10.1039/b000000x/

‡ Footnotes should appear here. These might include comments relevant to but not central to the matter under discussion, limited experimental and spectral data, and crystallographic data.

[1] J. B. Goodenough and K.-S. Park. *J. Am. Chem. Soc.*, 2013, **135**, 1167.

[2] N-S. Choi, Z. H. Chen, S. A. Freunberger, X. L. Ji, Y-K. Sun, K. Amine, G. Yushin, L. F. Nazar, J. Cho and P. G. Bruce, *Angew. Chem. Int. Ed.*, 2012, **51**, 2.

[3] Q. F. Zhang, E. Uchaker, S. L. Candelariaza and G. Z. Cao, *Chem. Soc. Rev.*, 2013, **42**, 3127.

[4] M. K. Song, S. Park, F. M. Alamgir, J. Cho and M. L. Liu, *Mater. Sci. Eng., R*, 2011, **72**, 203.

[5] P. Poizot, S. Laruelle, S. Grugeon, L. Dupont and J. M. Tarascon, *Nature*, 2000, **407**, 496.

[6] Z. Y. Wang, L. Zhou and X. W. Lou, *Adv. Mater.*, 2012, **24**, 1903.

[7] J. N. Tiwari, R. N. Tiwari and K. S. Kim, *Prog. Mater. Sci.*, 2012, **57**, 724.

[8] D. R. Rolison, J. W. Long, J. C. Lytle, A. E. Fischer, C. P. Rhodes, T. M. McEvoy, M. E. Bourg and A. M. Lubers, *Chem. Soc. Rev.*, 2009, **38**, 226.

[9] A. J. Mieszawska, R. Jalilian, G. U. Sumanasekera and F. P. Zamborini. *Small*, 2007, **3**, 722.

[10] H. Y. Sun, Y. L. Yu, J. Luo, M. Ahmad and J. Zhu, *CrystEngComm*, 2012, **14**, 8626.

[11] H. Y. Sun, M. Ahmad and J. Zhu, *Electrochimica Acta*, 2013, **89**, 199.

[12] Y. L. Yu, X. L. Wang, H. Y. Sun and M. Ahmad, *RSC Advances*, 2012, **2**, 7901.

[13] H. B. Wu, H. Pang and X. W. Lou, *Energy Environ. Sci.*, 2013, **6**, 3619.

[14] M. H. Kim, Y. J. Hong and Y. C. Kang, *RSC Adv.*, 2013, **3**, 13110.

[15] Y. J. Hong, M.Y. Son and Y.C. Kang, *Adv. Mater.*, 2013, **25**, 2279.

[16] L. Zhou, D.Y. Zhao and X.W. Lou, *Adv. Mater.*, 2012, **24**, 745.

[17] L. Hu, H. Zhong, X.R. Zheng, Y.M. Huang, P. Zhang and Q.W. Chen, *Sci. Rep.*, 2012, **2**, 986.

[18] J. Cabana, L. Monconduit, D. Larcher and M.R. Palacín, *Adv. Mater.*, 2010, **22**, E170.

[19] P. Lavela, G.F. Ortiz, J.L. Tirado, E. Zhecheva, R. Stoyanova and Sv. Ivanova, *J. Phys. Chem. C*, 2007, **111**, 14238.

[20] Y. Y. Liang, H. L. Wang, J. G. Zhou, Y. G. Li, J. Wang, T. Regier and H. J. Dai, *J. Am. Chem. Soc.*, 2012, **134**, 3517.

[21] J. F. Li, S. L. Xiong, X. W. Li and Y. T. Qian, *Nanoscale*, 2013, **5**, 2045.

[22] C. Yuan, H. B. Wu, Y. Xie, X. W. Lou, *Angew. Chem. Int. Ed.*, 2014, **53**, 1488.

[23] L. Yu, L. Zhang, H. B. Wu, G. Zhang, X. W. Lou, Energy Environ. Sci., 2013,6, 2664-2671.

[24] C. Z. Yuan, J. Y. Li, L. R. Hou, X. G. Zhang, L. F. Shen and X. W. Lou, *Adv. Funct. Mater.*, 2012, **22**, 4592.

[25] G. Q. Zhang, H. B. Wu, H. E. Hoster, M. B. Chan-Park and X. W. Lou, *Energy Environ. Sci.*, 2012, **5**, 9453.

[26] Q. F. Wang, B. Liu, X. F. Wang, S. H. Ran, L. M. Wang, D. Chen. and G. Z. Shen, *J. Mater. Chem.*, 2012, **22**, 21647.

[27] M. C. Liu, L. B. Kong, C. Lu, X. M. Li, Y. C. Luo and L. Kang, *ACS Appl. Mater. Interfaces*, 2012, **4**, 4631.

[28] X. H. Lu, X. Huang, S. L. Xie, T. Zhai, C. S. Wang, P. Zhang, M. H. Yu, W. Li, C. L. Liang and Y. X. Tong, *J. Mater. Chem.*, 2012, **22**, 13357.

[29] J. Chang, J. Sun, C. H. Xu, H. Xu and L. Gao, *Nanoscale*, 2012, **7**, 6786.

[30] Y. J. Feng, R. Q. Zou, D. G. Xia, L. L. Liu and X. D. Wang, *J. Mater. Chem. A*, 2013, **1**, 9654.

[31] Y. M. Sun, X. L. Hu, W. Luo and Y. H. Huang, *J. Mater. Chem.*, 2012, **22**, 13826.

[32] B. D. Chen, C. X. Peng and Z. Cui, *Trans. Nonferrous Met. Soc.* China, 2012, **22**, 2517.

[33] M. A. Peck and M. A. Langell, *Chem. Mater.*, 2012, **24**, 4483.

[34] Q. M. Pan and J. Liu, *J. Solid State Electrochem.*, 2009, **13**, 1591.

[35] X. Li, A. Dhanabalan, K. Bechtold and C. Wang, *Electrochem. Commun.*, 2010, **12**, 1222.

[36] C. Wang, D. Wang, Q. Wang and H. Chen, *J. Power Sources*, 2010, **195**, 7432.

[37] X. H. Wang, L. Qiao, X. L. Sun, X. W. Li, D. K. Hu, Q. Zhang and D. Y. He, *J. Mater. Chem. A*, 2013,**1**, 4173.

[38] J. Jiang, J. P. Liu, R. M. Ding, X. X. Ji, Y. Y. Hu, X. Li, A. Z. Hu, F. Wu, Z. H. Zhu and X. T. Huang, *J. Phys. Chem. C*, 2010, **114**, 929.

[39] Y.M. Wang, X. Zhang, C.Y. Guo, Y. Q. Zhao, C. L. Xu,and H. L. Li, *J. Mater. Chem. A*, 2013, **1**, 13290.

Graphical Abstract

Mesoporous $CoNiO_2$ structures can be considered an alternative material for the applications in the design of energy storage devices.